Research Square

Preprints are preliminary reports that have not undergone peer review.
They should not be considered conclusive, used to inform clinical practice,
or referenced by the media as validated information.

Mesenchymal Stem Cells Promote Healing of Radiation-Induced Skin Injury by Enhancing Mitochondrial Function

Guanyan He
Guiyang Medical University
Yang Xu
Army Medical University
Wenfeng Li
Army Medical University
Xiaorui Shi
Southwest Hospital
Xueli Pan
Guiyang Medical University
Chunmeng Shi
shicm@tmmu.edu.cn

Guiyang Medical University

Research Article

Keywords: Human umbilical cord mesenchymal stem cells, Radiation-induced skin injury, Mitochondria, Fibroblasts, Wound healing

Posted Date: March 9th, 2026

DOI: https://doi.org/10.21203/rs.3.rs-8438584/v1

License: This work is licensed under a Creative Commons Attribution 4.0 International License.
Read Full License

Additional Declarations: No competing interests reported.

Abstract

Background Human umbilical cord mesenchymal stem cells (HUCMSCs) are attractive for tissue repair because of their broad availability, low immunogenicity, and limited ethical constraints. However, the mechanisms by which HUCMSCs mitigate radiation-induced skin injury, particularly effects on fibroblast mitochondrial function and energy metabolism, remain incompletely defined.

Methods We investigated the effects of HUCMSCs on irradiated fibroblasts *in vitro* and in a murine model of radiation-induced skin injury. *In vitro*assays evaluated fibroblast proliferation, migration, mitochondrial membrane potential, cellular respiration, and ATP production, and assessed intercellular mitochondrial transfer. *In vivo*, local subcutaneous administration of HUCMSCs was applied to the radiation-injured skin in male C57BL/6J mice; wound closure, inflammatory marker expression, oxidative stress, angiogenesis, and extracellular matrix deposition were evaluated.

Results *In vitro*, HUCMSCs markedly enhanced proliferation and migration of irradiated fibroblasts and restored mitochondrial membrane potential, respiration, and ATP synthesis; intercellular mitochondrial transfer contributed to these effects. In the murine model, local HUCMSC treatment significantly accelerated wound closure, decreased expression of inflammatory markers, attenuated oxidative stress, and promoted angiogenesis and extracellular matrix deposition in injured skin.

Conclusions HUCMSCs alleviate radiation-induced skin damage by remodeling fibroblast mitochondrial function and restoring cellular energy metabolism. These findings provide experimental support for mitochondria-targeted, cell-based therapies as a potential strategy to prevent or treat radiotherapy-associated skin toxicity.

1. Introduction

Radiotherapy plays an irreplaceable role in the treatment of malignant tumors, but it can also cause irreversible damage to normal skin[1]. Radiation-induced skin injury (RISI) is one of the most common complications of radiotherapy[2], with clinical manifestations ranging from acute erythema, desquamation, moist exudation, and ulceration[3, 4], to chronic hyperpigmentation, skin atrophy, telangiectasia, fibrosis, and non-healing ulcers[5]. Chronic, refractory wounds are often accompanied by persistent pain and recurrent infections, severely compromising patients' quality of life[6], and limiting the dose and duration of radiotherapy, thereby posing a major challenge for long-term patient management[7].

Ionizing radiation not only directly induces DNA damage in tissues and cells but also generates large amounts of reactive oxygen species (ROS), triggering sustained oxidative stress[8], that damages cellular membranes, proteins, and nucleic acids[9]. Mitochondria are central targets of radiation and oxidative stress: radiation can disrupt the mitochondrial electron transport chain, leading to excessive ROS production, loss of membrane potential, reduced adenosine triphosphate (ATP) generation, and increased apoptosis and necrosis[10–12]. At the same time, mitochondrial damage further exacerbates

oxidative stress, thereby amplifying mitochondrial dysfunction[13]. In addition to disrupting mitochondrial function, radiation induces the sustained release of inflammatory cytokines such as TNF-α, IL-1β, and IL-6[14], maintaining the local wound in a state of chronic inflammation and oxidative stress and markedly impairing tissue repair[15–18]. Consequently, there is an urgent need to develop novel therapeutic strategies that can attenuate oxidative stress, restore mitochondrial function, and modulate inflammation.

Current treatment options for radiation-induced skin injury mainly include topical agents such as glucocorticoids[19], moisturizers[20], anti-infective preparations[21], and growth factor-based formulations[22], as well as hyperbaric oxygen therapy[23]. These approaches can alleviate symptoms and promote granulation tissue formation to some extent[4], but are largely limited to local supportive care[24], and do not effectively target underlying mechanisms such as mitochondrial damage and sustained oxidative stress, resulting in suboptimal outcomes for chronic, non-healing radiation-induced wounds. In recent years, regenerative medicine and cell-based therapies have provided new strategies for the management of radiation-induced tissue injury. Mesenchymal stem cells (MSCs) not only possess multilineage differentiation potential[25], but also secrete growth factors and cytokines[26], that modulate inflammatory responses, promote angiogenesis, and remodel the wound microenvironment, thereby exhibiting promising pro-repair effects in various refractory wounds[27].

Among human mesenchymal stem cells, human umbilical cord mesenchymal stem cells (HUCMSCs) are considered a highly promising cell source because of their wide availability, ease of collection, low immunogenicity, and relatively minor ethical concerns[28]. Studies have shown that HUCMSCs improve the blood supply and inflammatory microenvironment of injured tissues by secreting growth factors such as VEGF, HGF, and bFGF, as well as anti-inflammatory cytokines[29], in addition, their secreted exosomes are enriched in multiple functional proteins and microRNAs that promote target-cell proliferation, migration, and resistance to apoptosis[30]. Furthermore, HUCMSCs have been shown to transfer functional mitochondria to damaged cells via intercellular connections, thereby improving cellular energy metabolism, reducing ROS levels, and enhancing cell survival[31, 32]. For radiation-induced skin-wound cells characterized by heightened oxidative stress and mitochondrial dysfunction, HUCMSCs therefore have important potential advantages. For radiation-induced skin-wound cells characterized by heightened oxidative stress and mitochondrial dysfunction, HUCMSCs therefore have important potential advantages.

Fibroblasts are key effector cells in cutaneous wound healing, responsible for extracellular matrix synthesis, granulation tissue formation, and wound contraction[33], their proliferative and migratory capacities directly determine healing quality and rate[34]. Radiation injury markedly suppresses fibroblast proliferation and migration[35], and induces mitochondrial dysfunction and apoptosis in these cells[36, 37], thereby contributing to persistent wound nonclosure. Therefore, targeted restoration of mitochondrial function and reduction of oxidative stress in radiation-damaged fibroblasts may represent a critical strategy to enhance the repair of radiation-induced skin wounds.

Based on the above, this study investigates the therapeutic effects and underlying mechanisms of HUCMSCs in radiation-induced skin injury. We hypothesize that HUCMSCs promote proliferation and migration of murine fibroblasts and improve the local wound microenvironment. In addition, HUCMSCs may restore and enhance fibroblast mitochondrial function-for example *via* intercellular mitochondrial transfer— thereby synergistically attenuating inflammation and oxidative stress and substantially accelerating the repair of radiation-induced skin wounds. This work aims to provide new strategies and mechanistic evidence to support cell-based therapies for radiation-induced skin injury.

2. Materials and Methods

2.1 Skin tissue RNA sequencing

Ten male C57BL/6J mice (8 weeks old) were purchased from the Experimental Animal Center of the Army Medical University (Third Military Medical University). The animals were randomly assigned to cages and acclimatized for 1 week under controlled temperature and natural ventilation conditions prior to subsequent experiments. Protocols for animal experiments were approved by the Laboratory Animal Welfare and Ethics Committee of the Army Medical University (AMU; Approval No. AMUWEC20230024). The project “Mechanistic study of transcription coactivator PC4 negatively regulating Sitt3 transcription and inhibiting the healing of radiation-induced skin ulcers” (Approval No. AMUWEC20230024) was approved by the Laboratory Animal Welfare and Ethics Committee of the Army Medical University on 2 December 2023. All animal experiments conducted in this study were carried out in accordance with the ARRIVE 2.0 guidelines and the relevant institutional regulations. Mice were anesthetized with sodium pentobarbital (intraperitoneal injection, 60 mg/kg), and dorsal hair was removed. Mice were allocated to experimental groups using a random number table. The dorsal irradiation area of each mouse received a single dose of 20 Gy (dose rate 0.9 Gy/min) of X-rays. Skin tissue samples were collected at days 14 after euthanizing the mice by overdose of sodium pentobarbital (intraperitoneal injection, 150 mg/kg) and non-irradiated controls (n = 5). Samples were submitted to Majorbio Biotech for transcriptome sequencing. The workflow included total RNA extraction and assessment of RNA purity and concentration, transcriptome library preparation, and sequencing on an Illumina NovaSeq X Plus platform. Following sequencing, data were subjected to Gene Ontology (GO) and Kyoto Encyclopedia of Genes and Genomes (KEGG) enrichment analyses to identify functions and pathways associated with differentially expressed genes.

2.2 Source and Culture Conditions of HUCMSCs and L929

Human umbilical cord-derived mesenchymal stem cells (HUCMSCs) were purchased from the American Type Culture Collection (ATCC, USA, Cat PCS-500-010 ™). These cells met all criteria defined by the International Society for Cellular Therapy (ISCT) for classification as mesenchymal stem cells (MSCs). HUCMSCs at passage 3 (P3) were cultured in α-minimum essential medium (α-MEM; Thermo Fisher Scientific) supplemented with 10% fetal bovine serum (FBS; Gibco) and maintained at 37°C in a humidified incubator containing 5% CO_2.

The L929 cells line was purchased from Servicebio (Cat STCC20025P), cultured in Dulbecco's Modified Eagle Medium (DMEM; Gibco) supplemented with 10% horse serum (Gibco) and maintained at 37°C in a humidified incubator containing 5% CO_2.

2.3 Flow cytometry

HUCMSCs were characterized by flow cytometry (BD FACS). Cells were cultured in Procell human umbilical cord mesenchymal stem cell complete medium (Procell, [Cat CM-CL11]) to 90% confluence, detached with trypsin, and resuspended at a concentration of 1×10^6 cells/mL. Aliquots of 100 µL cell suspension were dispensed into seven 1.5 mL Eppendorf tubes. Cells were washed with 1 mL PBS and centrifuged at 300 g for 5 min. After discarding the supernatant, aliquots were incubated with antibodies against CD90, CD73, CD105, CD34, CD44, and HLA-DR, one tube received PBS only and served as the unstained (blank) control. Tubes were incubated in the dark at 4 ℃ for 30 min. Following incubation, cells were washed with PBS to remove unbound antibody and analyzed on a BD FACS flow cytometer for surface marker expression.

2.4 Characterization of HUCMSCs

When cultures reached approximately 80% confluence, the standard HUCMSC medium was replaced with either Procell adipogenic induction medium or Procell osteogenic induction medium according to the manufacturer’s instructions. Cells were maintained in the respective induction media for day 21, with medium changes every 3 days. Samples were collected at day 7 and day 21. Adipogenic differentiation was assessed by Oil Red O staining, and osteogenic differentiation was assessed by Alizarin Red S staining, with imaging performed by light microscopy.

2.5 Construction of the HUCMSC-L929 Transwell co-culture system

A Transwell co-culture system was established to evaluate the effects of human umbilical cord mesenchymal stem cells (HUCMSCs) on irradiated murine fibroblasts (L929). Transwell inserts with an 8 µm pore size (Corning, [Cat3422]) were used. HUCMSCs were seeded in the upper chamber, and L929 cells were seeded in the lower chamber. After cell attachment, L929 cells in the lower chamber were irradiated with X-rays (total dose 6 Gy; dose rate 0.9 Gy/min) and immediately co-cultured with HUCMSCs in the upper chamber under standard culture conditions. Co-culture durations are specified in the descriptions of individual assays below. Experiments were performed with at least three independent biological replicates (n = 3).

2.6 Colony formation assay

L929 cells were seeded in 6-well plates at an initial density of 1×10^3 cells/well. Co-culture conditions followed section 2.4. Cells were co-cultured for 7 days or until colonies were visible. Colonies were fixed with 4% paraformaldehyde for 15 min, washed with distilled water, and stained with 0.1% crystal violet for 20 min. Plates were washed with distilled water and air-dried. Colonies containing more than 50 cells

were counted under a stereomicroscope. Data were obtained from three independent biological replicates, each with three technical wells per group.

2.7 Cell Counting Kit-8 (CCK-8) assay

L929 cells were seeded in 24-well plates at an initial density of 2×10^4 cells/well. After cell attachment, cells were irradiated (6 Gy, 0.9 Gy/min) according to group assignment. For the co-culture group, HUCMSCs were placed in Transwell inserts as specified in 2.4. Cell viability was evaluated on day 1, 2 and 3 post-irradiation using the Cell Counting Kit-8 (CCK-8, Beyotime, [CatC0039]). CCK-8 reagent was added according to the manufacturer's instructions and plates were incubated at 37 ℃ for 2 h. Absorbance was measured at 450 nm using a microplate reader. Viability and membrane integrity were also assessed by Calcein-AM/PI (Calcein-AM/PI, Beyotime, [CatC2015M]) double staining and fluorescence microscopy.

2.8 Scratch assay and Transwell migration assay

Scratch assay: L929 cells were seeded in 6-well plates at 2×10^5 cells/well and cultured to approximately 80% confluence. The IR and HUCMSC + IR groups were irradiated (6 Gy, 0.9 Gy/min). Immediately after irradiation, a linear scratch was made through the monolayer using a sterile 200 μL pipette tip. Debris and detached cells were removed by washing with PBS, and cells were cultured in RPMI 1640 containing 1% FBS to suppress proliferation and permit assessment of migration. For co-culture, HUCMSCs were placed in Transwell inserts above the L929 monolayers. Images of the wound area were acquired at 0, 12 and 24 h with an inverted microscope and wound areas were measured with ImageJ; relative migration at 24 h was expressed as the percentage reduction in wound area versus 0 h (n = 3).

Transwell migration assay: Cell suspensions from each treatment group were placed into the upper chamber of Transwell inserts in 24-well plates (pore size 8 μm, Corning, [Cat3422]). For HUCMSC co-culture groups, HUCMSCs were seeded in the lower chamber. After 24 h incubation, non-migrated cells on the upper membrane surface were removed with a cotton swab. Migrated cells on the lower membrane surface were fixed with 4% paraformaldehyde for 15 min, stained with 0.1% crystal violet for 20 min, washed with PBS, imaged, and counted under a light microscope.

2.9 Reactive oxygen species (ROS) measurement

L929 cells were seeded at 2×10^5 cells/well in 6-well plates. After irradiation (6 Gy, 0.9 Gy/min), cells were incubated for 6 h and then stained with 2',7'-dichlorodihydrofluorescein diacetate (DCFH-DA, solarbio, [CatCA1410]) according to the manufacturer's instructions (incubate 30 min at 37 ℃ in the dark). Excess probe was removed by washing cells three times with PBS. ROS production was observed under a fluorescence microscope and quantified by flow cytometry.

2.10 JC-1 staining for mitochondrial membrane potential

L929 cells were seeded at 1×10^5 cells/well in 12-well plates and treated per group. Forty-eight hours after irradiation, cells were washed twice with PBS and incubated with JC-1 staining solution (Servicebio,

[CatG1515]) at 37 ℃ for 30 min following the manufacturer's instructions. After two PBS washes, cells were imaged by fluorescence microscopy. The ratio of red to green fluorescence intensity (aggregate/monomer) was calculated by ImageJ to indicate changes in mitochondrial membrane potential.

2.11 Intracellular ATP measurement

L929 cells were seeded at 1×10^5 cells/well in 12-well plates and treated as described. At 48 h post-irradiation, cells were washed with PBS, trypsinized, and counted. Cell suspensions were adjusted to equal cell numbers across groups. Aliquots of 100 μL cell suspension were transferred to 96-well white plates and ATP assay working solution was added according to the kit protocol (Chemiluminescence, DongRren, [CatCK18]). ATP levels were measured using a chemiluminescence plate reader. A standard curve prepared with ATP standards was used to calculate absolute ATP concentrations. Each condition was assayed in triplicate (n = 3).

2.12 Transmission electron microscopy (TEM)

L929 cells were seeded at 3×10^5 cells/well in 6-well plates and treated per protocol. At 48 h post-irradiation, cells were washed with PBS, scraped, and fixed in 2.5% glutaraldehyde at 4℃ overnight. Standard TEM sample processing (post-fixation, dehydration, embedding, ultrathin sectioning and staining with uranyl acetate/lead citrate) was performed. Ultrastructural imaging was performed with a transmission electron microscope (n = 3).

2.13 Live confocal fluorescence imaging of mitochondria transfer

The lentiviral construct lenti-CMV-mito-eGFP-PGK-Puro (Genomeditech) was used to express the mitochondria-targeted fusion protein mito-eGFP under the control of a CMV promoter. The fusion protein contains a mitochondrial targeting sequence that directs mito-eGFP to mitochondria, rendering them fluorescently green. HUCMSCs transduced and selected for mito-eGFP expression were co-seeded with L929 cells on glass-bottom dishes suitable for live-cell imaging. Time-lapse imaging was performed on a super-resolution confocal microscope with environmental control (temperature and CO_2) for 48 h.

2.14 Murine radiation-induced skin injury model and treatments

Twenty male C57BL/6J mice (8 weeks old) were purchased from the Experimental Animal Center of the Army Medical University. The housing conditions, grouping method, and irradiation modeling procedures for the mice were the same as those described in Section 2.1. Animals were randomized into IR and HUCMSCs treatment groups (n = 10 per group). On day 7 post-irradiation, a 6 mm full-thickness circular skin wound was created at the irradiated site using a sterile biopsy punch. IR group wounds were injected with 100 μL saline and covered with sterile 3M wound dressing. In the HUCMSCs group, 2×10^6 HUCMSCs in 100 μL saline were injected subcutaneously around the wound margin within 2 h after

wound creation; the wound was then covered with sterile 3M dressing. Wound area photographs were recorded on days 0, 3, 7 and 14 after treatment. Blood samples for biosafety assessment were collected on days 7. For tissue harvesting, mice were euthanized by sodium pentobarbital injection (intraperitoneal injection, 60 mg/kg), and skin tissue samples were then collected on days 7 and 14 for histological and molecular analyses.

2.15 Histological staining

Skin tissue samples collected at day 7 and day 14 post-irradiation were fixed in 4% paraformaldehyde for > 24 h, processed for paraffin embedding, and sectioned at 4μm thickness. Sections were deparaffinized, rehydrated and stained with hematoxylin and eosin (H&E) and Masson's trichrome according to standard protocols to assess histopathological changes and collagen deposition. Stained sections were examined and imaged under a light microscope; images were used for qualitative assessment and quantitative analysis.

2.16 Immunofluorescence

Paraffin sections were deparaffinized, rehydrated and subjected to antigen retrieval in citrate buffer (pH 6.0) by microwave method. Sections were blocked with 5% goat serum at room temperature for 1 h to reduce nonspecific binding. Primary antibodies (Ki-67, CD31, Arg-1, iNOS) were applied and incubated overnight at 4 ℃. After PBS washes, sections were incubated with fluorescently labeled secondary antibodies at room temperature for 1 h, followed by nuclear counterstaining with DAPI (8 min, RT). Slides were mounted and imaged using a confocal microscope (Olympus FV3000, n = 3).

2.17 Enzyme-linked immunosorbent assay (ELISA)

Protein levels of TNF-α, IL-6, IL-10 and IL-4 in skin tissue homogenates were quantified using commercial ELISA kits according to the manufacturers' protocols: mouse TNF-α ELISA kit (MeiKe, [CatMK2868A]), mouse IL-6 ELISA kit (Elabscience, [CatE-EL-M0044]), mouse IL-10 ELISA kit (Elabscience, [CatE-EL-M0046]) and mouse IL-4 ELISA kit (FineTest, [CatEM0119).

2.18 Statistical analysis

Statistical analyses were conducted using GraphPad Prism version 9. For comparisons between two groups, an unpaired two-tailed *Student's* t-test was used if data were normally distributed. For multiple group comparisons, one-way analysis of variance (ANOVA) followed by Tukey's post hoc test was applied. For experiments involving two independent variables, two-way ANOVA followed by Tukey's multiple comparisons test was used. Normality was tested using the Shapiro-Wilk test where appropriate. A p value < 0.05 was considered statistically significant.

3. Results

3.1 Mechanistic Analysis of Radiation-Induced Cutaneous Injury

To investigate the molecular mechanisms underlying radiation-induced skin injury, we established a mouse model of radiation-induced skin injury and performed RNA-seq on irradiated (IR) and corresponding normal skin (Normal) samples. Differential expression analysis identified 3,392 genes that were significantly altered between IR and Normal groups (fold change ≥ 2, $p < 0.05$; Fig. 1A,B), of which 1,594 were upregulated and 1,798 were downregulated in IR. Gene Ontology (GO) enrichment analysis (Fig. 1C) revealed that DEGs in the IR group were significantly enriched in biological processes such as response to oxidative stress and inflammatory response, indicating a close association between radiation injury, oxidative stress, and immune/inflammatory activation. KEGG pathway analysis (Fig. 1D) showed significant enrichment in pathways related to cellular stress, energy metabolism, and cell-fate regulation, including NF-κB signaling, Glycolysis/Gluconeogenesis, Toll-like receptor signaling, Apoptosis, ROS-related pathways, and Oxidative phosphorylation. Representative genes contributing to these enrichments included Il1b, Il6, Tnf, Cxcl1, Ccl2, Hmox1, Txnrd1, Pink1, Sqstm1, Fundc1, Sdha, and mt-Atp6. The enrichment patterns suggest that radiation-induced oxidative damage, inflammatory signaling, mitochondrial dysfunction, and apoptosis may act together to drive the development and progression of radiation-induced skin injury.

3.2 Characterization of HUCMSCs

Phenotypic analysis of HUCMSCs was performed by flow cytometry (Fig. S1A). The cells were positive for mesenchymal markers CD90, CD73 and CD105, each with a positivity rate of at least 95%, and negative for hematopoietic/immune markers CD34, CD44 and HLA-DR, each with expression below 1%, meeting the internationally accepted criteria for mesenchymal stromal cells and validating their use in subsequent experiments. A defining biological property of HUCMSCs is their multipotent differentiation capacity. Under lineage-specific induction conditions *in vitro*, HUCMSCs can differentiate into adipogenic, osteogenic and chondrogenic lineages. As a routine validation of multipotency, adipogenic induction followed by Oil Red O staining revealed prominent intracellular lipid droplets that increased in number with prolonged induction (Fig. S1B,C). Osteogenic induction produced mineralized nodules that stained strongly with Alizarin Red S, with nodule number increasing over time (Fig. S1D,E). These data confirm that the HUCMSCs used in this study display canonical MSC surface marker expression and multipotent differentiation potential suitable for downstream functional assays.

3.3 HUCMSCs Enhance Proliferation and Migration of Irradiated L929 Cells *in vitro*

To evaluate whether HUCMSCs mitigate irradiation-induced suppression of L929 cell proliferation, colony formation assays were performed. The colony formation assay showed that irradiated (IR) cells produced significantly fewer and smaller colonies compared with controls, indicating impaired proliferative and self-renewal capacity (Fig. 2B,C). Co-culture with HUCMSCs substantially increased both colony number and colony size relative to the IR group, demonstrating that HUCMSCs promote post-irradiation cell proliferation. Cell viability assessed by Calcein-AM/PI staining corroborated these findings: the HUCMSC group exhibited a markedly higher survival rate than the IR group (Fig. 2D). CCK-8

assays produced consistent results (Fig. 2E). Because cell migration is critical for wound healing, scratch assays were used to test whether HUCMSCs enhance migration of irradiated cells. HUCMSC treatment significantly increased wound closure at 24 h compared with IR alone (Fig. 2F,G). Transwell migration assays further confirmed that HUCMSCs effectively promoted migration of irradiated L929 cells (Fig. 2H,I). Together, these *in vitro* data indicate that HUCMSCs facilitate both proliferation and migration of L929 cells after irradiation.

3.4 HUCMSCs mitigate irradiation-induced oxidative stress injury

To evaluate whether HUCMSCs protect L929 cells from irradiation-induced oxidative stress, intracellular reactive oxygen species (ROS) levels were assessed using the fluorescent probe DCFH-DA. DCFH-DA is hydrolyzed intracellularly and oxidized by ROS to fluorescent DCF (green). Fluorescence microscopy revealed that DCF intensity was markedly reduced in the HUCMSCs co-culture group compared with the irradiated (IR) group (Fig. 3A,B), indicating suppression of irradiation-induced ROS production; flow cytometric quantification confirmed these findings (Fig. 3C,D).

Excessive ROS induce structural and functional mitochondrial damage, disrupt electron transport chain activity, and consequently diminish cellular ATP synthesis. Measurement of intracellular ATP showed that irradiation significantly decreased ATP levels in L929 cells, whereas co-culture with HUCMSCs partially restored ATP production (Fig. 3E). Mitochondrial dysfunction is also accompanied by loss of mitochondrial membrane potential (MMP). Using JC-1 staining, which forms red-emitting aggregates in polarized mitochondria and remains as green-emitting monomers in depolarized mitochondria, we observed predominant green fluorescence in the IR group but increased red signal in the HUCMSC group (Fig. 3F,G), indicating attenuation of irradiation-induced MMP loss by HUCMSCs.

Transmission electron microscopy (TEM) analysis revealed ultrastructural mitochondrial alterations: control cells displayed intact double membranes and well-organized cristae, whereas IR cells exhibited swollen cristae, widened intercristal spaces, matrix condensation, reduced and rounded mitochondria with disrupted cristae, features consistent with severe mitochondrial injury (Fig. 3H,I). Previous reports indicate that MSCs can rescue damaged cells by transferring healthy mitochondria, thereby improving respiration and energy metabolism. To investigate this mechanism, we labeled HUCMSCs mitochondria with mitochondria-targeted GFP and co-cultured them with irradiated L929 cells. Confocal imaging demonstrated GFP-labeled mitochondria originating from HUCMSCs and entering L929 cells (Fig. 3K,Video S1). Together, these results suggest that HUCMSCs alleviate irradiation-induced mitochondrial dysfunction in L929 cells by reducing ROS generation, restoring MMP, and preserving mitochondrial integrity.

3.5 HUCMSCs accelerate healing of radiation-induced skin wounds

To investigate the therapeutic effect and safety of HUCMSCs in radiation-induced skin wound healing, we established a mouse model by delivering a 20 Gy local dose to the dorsal skin and creating a 6 mm full-thickness circular wound in the irradiated area 7 days later. Mice were randomized to receive subcutaneous injections of either saline (control) or HUCMSCs. To evaluate systemic safety of local HUCMSCs administration, serum samples were collected on day 7 post-injection and analyzed for liver and kidney function markers including alkaline phosphatase (ALP), aspartate aminotransferase (AST), alanine aminotransferase (ALT), blood urea nitrogen (BUN), and creatinine (CREA). No significant elevations in these biomarkers were observed (Fig. 4B), indicating that subcutaneous HUCMSCs injection was well tolerated under the experimental conditions.

Wound areas were measured on day 3, 7 and 14 after wound creation to assess healing kinetics. The HUCMSCs-treated group exhibited significantly accelerated wound closure compared with controls (Fig. 4C,E). Specifically, the relative wound areas at day 3, 7 and 14 were 67.31%, 55.28% and 9.43% in the control group versus 62.29%, 48.93% and 4.68% in the HUCMSCs group, respectively (Fig. 5E).

Histological analyses corroborated the macroscopic findings: HUCMSCs treatment markedly enhanced epithelial regeneration, with greater epidermal thickness than controls (Fig. 4F,G). Masson's trichrome staining revealed increased collagen deposition in regenerated skin of the HUCMSCs group relative to controls, consistent with improved matrix remodeling (Fig. 4H,I). In summary, subcutaneous administration of HUCMSCs accelerates healing of radiation-induced skin wounds and enhances histological repair without detectable systemic hepatic or renal toxicity.

3.6 HUCMSCs promote wound healing, angiogenesis and exert anti-inflammatory effects in radiation-induced skin injury

To assess the effects of HUCMSCs on tissue regeneration and the immune microenvironment, we performed immunofluorescence staining and cytokine assays on wound tissues. Immunofluorescence revealed significantly higher expression of the endothelial marker CD31 and the proliferation marker Ki67 in HUCMSC-treated wounds compared with irradiated controls (IR) (Fig. 5A,B,E,F), indicating enhanced angiogenesis and cellular proliferation potentially associated with reduced oxidative stress.

To investigate immunomodulation, macrophage polarization markers were examined at day 7 post-wounding. Immunofluorescence showed elevated expression of the pro-inflammatory M1 marker iNOS in IR wounds, whereas iNOS signal was markedly reduced in the HUCMSC group; conversely, the M2 marker Arg1 was significantly upregulated following HUCMSC treatment (Fig. 5C,D,G,H). Quantitative analysis indicates that HUCMSCs promote a shift from M1 to M2 macrophage polarization, favoring inflammation resolution and tissue repair.

Consistent with these findings, ELISA measurements demonstrated that HUCMSC administration significantly decreased pro-inflammatory cytokines TNF-α and IL-6 while increasing anti-inflammatory

cytokines IL-4 and IL-10 (Fig. 5I). Together, these *in vivo* data suggest that HUCMSCs facilitate healing of radiation-induced skin wounds by enhancing angiogenesis and proliferation, driving macrophage polarization toward a reparative M2 phenotype, and modulating local inflammatory cytokine profiles.

4. Discussion

Radiation-induced skin injury (RISI) is a common and clinically significant complication of tumor radiotherapy[4], Non-healing wounds after irradiation largely result from persistent oxidative stress, chronic inflammation, and cellular dysfunction[38, 39], which together compromise patient quality of life and may interrupt oncologic treatment[40]. Therefore, there is an urgent need for therapeutic strategies that target these pathological processes. In this study, we demonstrate that HUCMSCs facilitate healing of radiation-induced skin wounds. *In vitro*, HUCMSCs markedly enhanced proliferation and migration of irradiated mouse fibroblasts. Mechanistically, our data indicate that HUCMSCs may alleviate mitochondrial dysfunction in irradiated cells via mitochondrial transfer, thereby improving cellular bioenergetics and viability. *In vivo*, local administration of HUCMSCs accelerated wound closure, modulated the inflammatory microenvironment, and promoted angiogenesis in a mouse model of RISI. Collectively, these findings suggest that HUCMSCs exert therapeutic effects through multi-modal actions, including restoration of cellular energy metabolism, attenuation of inflammation, and enhancement of regenerative cellular functions, supporting their potential for clinical translation. Nevertheless, several limitations remain: the precise molecular mediators of mitochondrial transfer need elucidation, long-term safety and efficacy require assessment, and optimization of dosing and delivery strategies warrants further investigation.

Wound healing is a complex, multi-stage process that includes inflammation, cellular proliferation and migration, extracellular matrix (ECM) synthesis, angiogenesis, and tissue remodeling[41]. The skin comprises three main layers, epidermis, dermis and hypodermis-each contributing distinct functions during repair[42]. Dermal fibroblasts are essential for ECM production and remodeling and play a central role in wound closure and restoration of tissue mechanics[43]. Previous studies have shown that mesenchymal stem cells (MSCs) facilitate tissue repair by secreting a repertoire of cytokines and growth factors, such as epidermal growth factor (EGF) and basic fibroblast growth factor (bFGF)[44, 45]. These factors exert anti-inflammatory, anti-apoptotic and pro-angiogenic effects and thereby regulate cell proliferation, differentiation and migration. In the present study, we found that HUCMSCs enhanced proliferation and migration of irradiated L929 fibroblasts; *in vitro* and *in vivo* corroborative data further support the contribution of HUCMSCs to wound repair, providing experimental rationale for their use in treating radiation-induced skin injury.

Previous studies have shown that ionizing radiation directly damages mitochondrial DNA and the electron transport chain, leading to mitochondrial dysfunction characterized by excessive reactive oxygen species (ROS) production, impaired ATP synthesis, and ultimately cellular senescence and apoptosis[46, 47]. Mitochondrial transfer is an intercellular process-either spontaneous or regulated-by which healthy cells deliver functional mitochondria to damaged cells *via* extracellular vesicles (EVs),

tunneling nanotubes, and other mechanisms to restore mitochondrial function[48–49]. Preclinical data indicate that exogenous mitochondria can integrate into recipient cells to enhance ATP generation, reestablish redox homeostasis, and improve cell survival under injurious conditions; analogous protective effects of MSC-mediated mitochondrial transfer have been reported in cardiomyocytes and alveolar epithelial cells[50–53]. Our findings support that HUCMSCs mitigate radiation-induced mitochondrial dysfunction in fibroblasts via mitochondrial transfer. Specifically, co-culture with HUCMSCs significantly reduced ROS levels in irradiated L929 cells, increased intracellular ATP production, and partially restored radiation-induced loss of mitochondrial membrane potential. Transmission electron microscopy demonstrated that HUCMSC treatment attenuated radiation-induced ultrastructural mitochondrial damage in L929 cells. Finally, confocal imaging of LUC-viral (lentiviral) labeled HUCMSC mitochondria in co-culture revealed transfer of mitochondria from HUCMSCs to irradiated L929 cells. Together, these data indicate that HUCMSCs may restore mitochondrial function and cellular bioenergetics in damaged cells by donating functional mitochondria, thereby reducing radiation-induced apoptosis and necrosis.

Motivated by the protective effects of HUCMSCs observed *in vitro*, we evaluated their therapeutic efficacy in a mouse model of radiation-induced skin injury (RISI). Local administration of HUCMSCs markedly enhanced wound healing: wound closure rates were significantly higher at all time points examined, and regenerated tissue exhibited a more intact epidermis, more abundant granulation tissue, and more organized collagen fiber architecture. Histological and immunohistochemical analyses indicated that HUCMSCs promoted angiogenesis and increased cellular proliferation within the wound. Given that persistent inflammation in RISI drives release of pro-inflammatory mediators, immune cell recruitment/activation, and exacerbation of tissue damage, we assessed inflammatory modulation by HUCMSCs. Treatment reduced levels of pro-inflammatory cytokines TNF-α and IL-6 while increasing anti-inflammatory cytokines IL-4 and IL-10. Phenotypic analysis further showed that HUCMSCs promoted macrophage polarization from a pro-inflammatory M1 phenotype ($iNOS^+$) toward a reparative M2 phenotype ($Arg1^+$). Taken together, HUCMSCs accelerate wound closure and suppress local inflammation while creating a pro-regenerative microenvironment, characterized by enhanced matrix deposition and neovascularization, that supports tissue remodeling and repair following radiation injury.

5. Conclusion

In summary, we demonstrate that human umbilical cord-derived mesenchymal stem cells (HUCMSCs) substantially accelerate the repair of radiation-induced skin injury by coordinating trophic support with mitochondrial rescue. HUCMSCs paracrine signaling enriches a pro-regenerative milieu, driving fibroblast proliferation and migration, promoting wound closure, tempering excessive inflammation, and facilitating matrix remodeling. In parallel, HUCMSCs restore mitochondrial homeostasis in radiation-damaged cells, consistent with mitochondria transfer-mediated recovery of cellular bioenergetics and stress tolerance. Together, these synergistic effects position HUCMSCs as a promising cell-based strategy for RISI and other refractory cutaneous wounds. Future work should define the molecular determinants and kinetics

of mitochondrial transfer, establish long-term efficacy and safety, and optimize dose, timing, and delivery routes to enable clinical translation.

Declarations

CRediT authorship contribution statement

Guangyan He: Writing-original draft, Data curation, Writing-review and editing. **Yang Xu:** Writing-review and editing, Resources, Methodology, Funding acquisition, Data curation. **Wenfeng Li**: Conceptualization. **Xiaorui Shi:** Investigation. **Xueli Pan:** Writing-review&editing. **Chunmeng Shi:** Writing-review and editing, Supervision, Resources, Funding acquisition, Conceptualization.

Data availability

The data used in this article is available from the corresponding author upon appropriate request.

Declaration of Competing Interest

The authors declare that they have no known competing financial interests or personal relationships that could have appeared to influence the work reported in this paper.

Acknowledgements

This work was financially supported by the National Natural Science Foundation of China (Nos.82192884, 82502271), Postdoctoral Innovation Talents Support Program of China (No. BX20230489) and NHC Key Laboratory of Nuclear Technology Medical Transformation (No. 2024HYX004). The authors declare that they have not use AI-generated work in this manuscript.

Ethics approval and consent to participate

Protocols for animal experiments were approved by the Laboratory Animal Welfare and Ethics Committee of the Army Medical University (AMU; Approval No. AMUWEC20230024). The project “Mechanistic study of transcription coactivator PC4 negatively regulating Sitt3 transcription and inhibiting the healing of radiation-induced skin ulcers” (Approval No. AMUWEC20230024) was approved by the Laboratory Animal Welfare and Ethics Committee of the Army Medical University on 2 December 2023. The work has been reported in line with the ARRIVE 2.0 guidelines.

References

1. Liu X, Guo T, Huang ZF, Chen S, Chen L, Li CY, et al. Acellular dermal matrix hydrogels promote healing of radiation-induced skin injury in a rat model. J Mater Chem B. 2024;12(43):11218–29.
2. Bentzen SM. Preventing or reducing late side effects of radiation therapy: radiobiology meets molecular pathology. Nat Rev Cancer. 2006;6(9):702–13.

3. Huang B, An L, Su WX, Yu DJ. Exploring the alterations and function of skin microbiome mediated by ionizing radiation injury. Front Cell Infect Microbiol. 2022;12:1029592.
4. Dadkhahfar S, Farokh P, Demehri S, Nazarian-Rosalynn M. Radiation-induced skin injury: mechanisms, clinical Manifestations, and management. Int J Dermatol. 2025;10:89.
5. Wilson Britney N, Shah R, Menzer C, Aleisa A, Kwong-Bernice Y. Consensus on the clinical management of chronic radiation dermatitis and radiation fibrosis: a Delphi survey. Br J Dermatol. 2022;187(6):1054–6.
6. Hao J, Sun MY, Li D, Li JY, Zhou DJ. An IFI6-based hydrogel promotes the healing of radiation-induced skin injury through regulation of the HSF1 activity. J Nanobiotechnol. 2022;20(1):288.
7. Wang YR, Yang L, Liu B, Liao S, Fu X, Zhou Y, et al. Radiation skin injury care in radiotherapy for oncology: mechanisms, drug therapy and novel biomaterial application strategies. Adv Ther. 2023;11:102–13.
8. Huangfu CJ, Tang N, Yang XK, Gong ZW, Huang Y, Ma YY. Improvement of irradiation-induced fibroblast damage by α2-macroglobulin through alleviating mitochondrial dysfunction. Pharm Biol. 2022;60(1):1365–73.
9. Fan PC, Zhang Y, Wang Y, Wei W, Zhou YX, Xie Y, et al. Quantitative proteomics reveals mitochondrial respiratory chain as a dominant target for carbon ion radiation: delayed reactive oxygen species generation caused DNA damage. Free Radic Biol Med. 2019;130:436–45.
10. Liu L, Li Y, Chen G, Chen Q. Crosstalk between mitochondrial biogenesis and mitophagy to maintain mitochondrial homeostasis. J Biomed Sci. 2023;30(1):86.
11. Du ZZ, Liu H, Huang X, Li Y, Wang TT, Liu J, et al. Design and synthesis of a mitochondria-targeting radioprotectant for promoting skin wound healing combined with ionizing radiation injury. Pharmaceuticals. 2022;15(6):721.
12. Dobler C, Jost T, Fietkau R, Distel L. Senescence induction by combined ionizing radiation and DNA damage response inhibitors in head and neck squamous cell carcinoma cells. Cells. 2020;9(9):1–9.
13. Baselet B, Driesen RB, Coninx E, et al. Rosiglitazone protects endothelial cells from irradiation-induced mitochondrial dysfunction. Front Pharmacol. 2020;11:268.
14. Sellin M-L, Koentopp LM, Bader R, Jonitz-Heincke A. Repeated exposure to CoCr28Mo6 particles leads to activation of NLRP3 inflammasome signaling in human osteoblasts. Cell Biol Toxicol. 2025;41(1):131.
15. Gudkov AV, Komarova EA. The role of p53 in determining sensitivity to radiotherapy. Nat Rev Cancer. 2003;3(2):117–29.
16. Yu CYY, Xu H, Ji S, Kwok RTK, Lam JWY, Li X et al. Mitochondrion-anchoring photosensitizer with aggregation-induced emission characteristics synergistically boosts the radiosensitivity of cancer cells to ionizing radiation. Adv Mater. 2017;29(15).
17. Averbeck D, Rodriguez-Lafrasse C. Role of mitochondria in IR responses: epigenetic, metabolic, and signaling impacts. Int J Mol Sci. 2021;22(20):11047.

18. J.Kim G, Chandrasekaran K, F.Morgan W. Mitochondrial dysfunction, persistently elevated levels of reactive oxygen species and radiation-induced genomic instability: a review. Mutagenesis. 2006;21(6):361–7.
19. Rosenthal A, Israilevich R, Moy R. Management of acute radiation dermatitis: a review of the literature and proposal for treatment algorithm. J Am Acad Dermatol. 2019;81(2):558–67.
20. Ghasemi A, Ghashghai Z, Akbari J, Yazdani-Charati J, Salehifar E, Hosseinimehr SJ. Topical atorvastatin 1% for prevention of skin toxicity in patients receiving radiation therapy for breast cancer: a randomized, double-blind, placebo-controlled trial. Eur J Clin Pharmacol. 2019;75(2):171–8.
21. Behroozian T, Goldshtein D, Wolf JR, Behroozian T, Goldshtein D, et al. MASCC clinical practice guidelines for the prevention and management of acute radiation dermatitis: part 1) systematic review. EClinicalMedicine. 2023;58:101886.
22. Lee J, Lee S, Hong JP, Shon MW, Ryu S-H, Ahn SD. Foam dressing with epidermal growth factor for severe radiation dermatitis in head and neck cancer patients. Int Wound J. 2014;13(3):390–3.
23. Hajikarimloo B, Kavousi S, Jahromi GG, Mehmandoost M, Oraee-Yazdani S, Fahim F. Hyperbaric oxygen therapy as an alternative therapeutic option for radiation-induced necrosis following radiotherapy for intracranial pathologies. World Neurosurg. 2024;186:51–61.
24. Xu Y, Liu Q, Li W, Hu Z, Shi C. Recent advances in the mechanisms, current treatment status, and application of multifunctional biomaterials for radiation-induced skin injury. Theranostics. 2025;15(7):2700–19.
25. Zhidu S, Ying T, Rui J, Chao Z. Translational potential of mesenchymal stem cells in regenerative therapies for human diseases: challenges and opportunities. Stem Cell Res Ther. 2024;15(1):266.
26. Han X, Liao R, Li X. Mesenchymal stem cells in treating human diseases: molecular mechanisms and clinical studies. Signal Transduct Target Ther. 2025;10(1):262.
27. Bharti D, Shivakumar SB, Park JK. Comparative analysis of human wharton's jelly mesenchymal stem cells derived from different parts of the same umbilical cord. Cell Tissue Res. 2017;372(1):51–65.
28. Mebarki M, Abadie C, Larghero J, Cras A. Human umbilical cord-derived mesenchymal stem/stromal cells: a promising candidate for the development of advanced therapy medicinal products. Stem Cell Res Ther. 2021;12(1):152.
29. Li J, Mao Q, He J, She H, Zhang Z, Yin C. Human umbilical cord mesenchymal stem cells improve the reserve function of perimenopausal ovary via a paracrine mechanism. Stem Cell Res Ther. 2017;8(1):55.
30. Li T, Yan Y, Wang B, et al. Exosomes derived from human umbilical cord mesenchymal stem cells alleviate liver fibrosis. Stem Cells Dev. 2013;22(4):845–54.
31. Boukelmoune N, Chiu GS, Kavelaars A, Heijnen CJ. Mitochondrial transfer from mesenchymal stem cells to neural stem cells protects against the neurotoxic effects of cisplatin. Acta Neuropathol Commun. 2018;6(1):139.

32. Liu K, Guo L, Zhou Z, Pan M, Yan C. Mesenchymal stem cells transfer mitochondria into cerebral microvasculature and promote recovery from ischemic stroke. Microvasc Res. 2019;123:74–80.
33. Wang Z, Cao K, Yan D. A study of the role of multiple layer-by-layer assembled bionic extracellular matrix in promoting wound healing via activation of the Wnt signaling pathway. J Biomed Mater Res Part B. 2023;111(1):1159–70.
34. Gharbia FZ, Abouhashem AS, Moqidem YA, Elbaz AA, Abdellatif A, SinghK, et al. Adult skin fibroblast state change in murine wound healing. Sci Rep. 2023;13(1):886.
35. Bainbridge P. Wound healing and the role of fibroblas. J Wound Care. 2013;22(8):407–12.
36. Sangsuwan T, Khavari AP, Blomberg, Godoy ED, Ringdahl MH. Oxidative stress levels and DNA repair kinetics in senescent primary human fibroblasts exposed to chronic low dose rate of ionizing radiation. Front Biosci-Landmark. 2023;28(11):296.
37. Bian XW, Piipponen MN, Liu Z, Chen YJ, Sangsuwan T, Maselli M, et al. Epigenetic memory of radiotherapy in dermal fibroblasts impairs wound repair capacity in cancer survivors. Nat Commun. 2024;15(1):9286.
38. Xia Y, Gui H, Li X, Wu Y, Liu J, Liu J. X-ray responsive antioxidant drug-free hydrogel for treatment of radiation skin injury. ACS Appl Mater Interfaces. 2025;17(4):5671–83.
39. Wang J, Xie K, Ren W, Han R, Xiao L, Wang YJ, et al. Huanglian jiedu plaster ameliorated X-ray-induced radiation dermatitis injury by inhibiting HMGB1-mediated macrophage-inflammatory interaction. J Ethnopharmacol. 2023;302:115917.
40. Kawamori J, Itaswa T, Fukushima S. A randomized controlled trial on the use of heparinoid moisturizer for improving quality of life with acute radiation skin damage from radiation therapy after breast-conserving surgery. Int J Radiat Oncol • Biol • Phys. 2019;105:E56.
41. Peña OA, Martin P. Cellular and molecular mechanisms of skin wound healing. Nat Rev Mol Cell Biol. 2024;25(8):599–616.
42. Gardeazabal L, Izeta A. Elastin and collagen fibres in cutaneous wound healing. Exp Dermatol. 2024;33(3):e15052.
43. Ryan JL. Ionizing radiation: the good, the bad, and the ugly. J Invest Dermatol. 2012;132(32):985–93.
44. Liu L, Yu Y, Hou Y. Human umbilical cord mesenchymal stem cells transplantation promotes cutaneous wound healing of severe burned rats. PLoS ONE. 2014;9(2):e88348.
45. Ma J, Zhang Z, Wang Y, Shen H. Investigation of miR-126-3p loaded on adipose stem cell-derived exosomes for wound healing of full-thickness skin defects. Exp Dermatol. 2021;31(3):362–74.
46. Ren Y, Yang P, Li C, Wang W, Zhang R, Li J, et al. Ionizing radiation triggers mitophagy to enhance DNA damage in cancer cells. Cell Death Discovery. 2023;9(1):267.
47. Livingston K, Schlaak RA, Puckett LL, Bergom C. The role of mitochondrial dysfunction in radiation-induced heart disease: from bench to bedside. Front Cardiovasc Med. 2020;7:20.

48. Dave KM, Stolz DB, Venna VR, Quaicoe VA, Maniskas ME, Reynolds MJ, et al. Mitochondria-containing extracellular vesicles (EV) reduce mouse brain infarct sizes and EV/HSP27 protect ischemic brain endothelial cultures. J Controlled Release. 2023;354:368–93.
49. Saha T, Dash C, Jayabalan R, Khiste S, Kulkarni A, Kurmi K, et al. Intercellular nanotubes mediate mitochondrial trafficking between cancer and immune cells. Nat Nanotechnol. 2021;17(1):98–106.
50. Huang T, Lin R, Su Y, Sun H, Zheng X, Zhang J, et al. Efficient intervention for pulmonary fibrosis via mitochondrial transfer promoted by mitochondrial biogenesis. Nat Commun. 2023;14(1):5781.
51. Kubat GB, Picone P, Tuncay E. Biotechnological approaches and therapeutic potential of mitochondria transfer and transplantation. Nat Commun. 2025;16(1):5709.
52. Liu K, Ji K, Guo L, Wu W, Lu H, Shan H, et al. Mesenchymal stem cells rescue injured endothelial cells in an in vitro ischemia-reperfusion model via tunneling nanotube like structure-mediated mitochondrial transfer. Microvasc Res. 2014;92:10–8.
53. Morrison TJ, Jackson MV, Cunningham EK. Mesenchymal stromal cells modulate macrophages in clinically relevant lung injury models by extracellular vesicle mitochondrial transfer. Am J Respir Crit Care Med. 2017;196(10):1275–86.

Figures

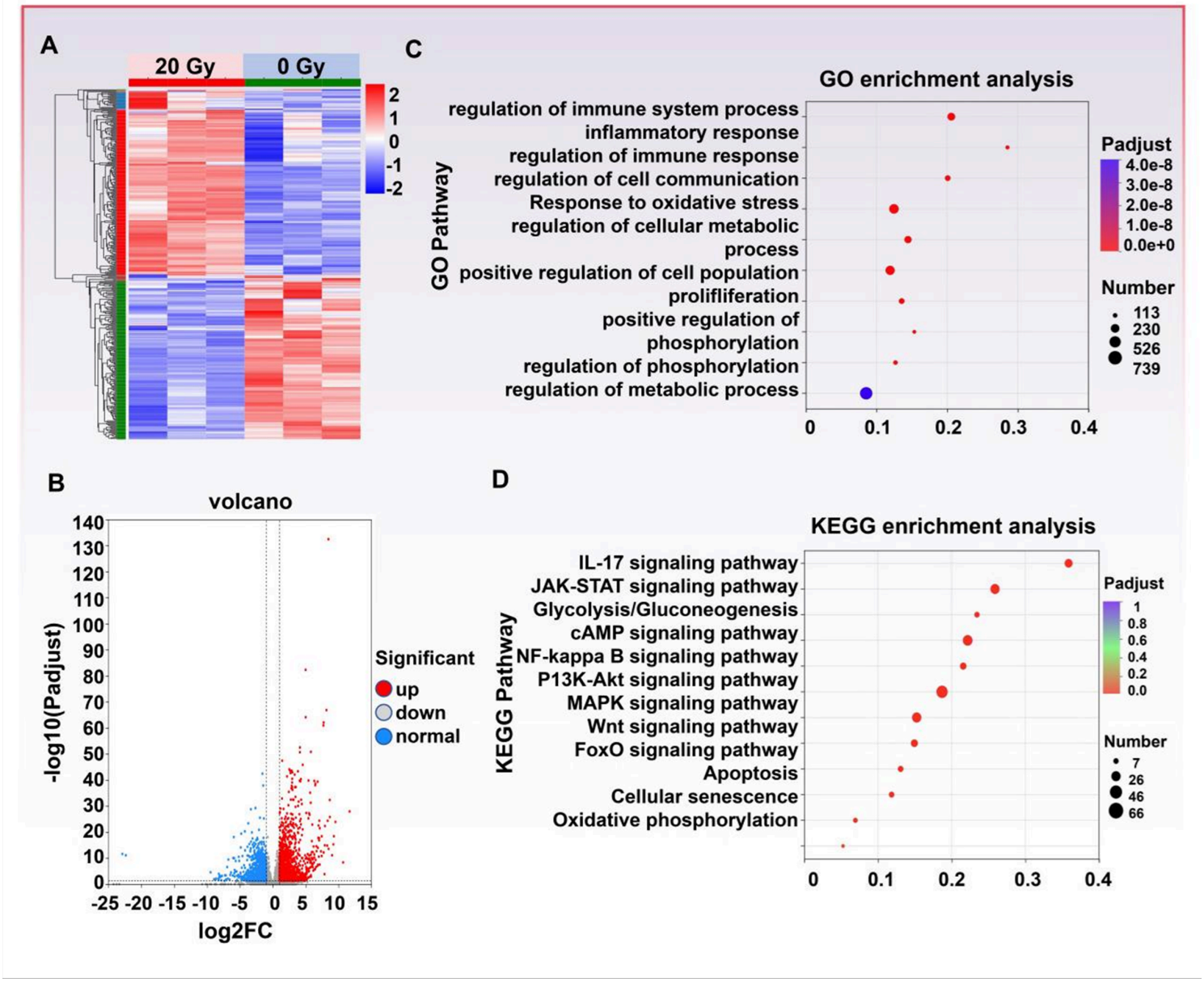

Figure 1

RNA-seq analysis of irradiated and normal skin. (**A**) Heatmap of differentially expressed mRNAs between irradiated (IR) and normal (Normal) skin. (**B**) Volcano plot showing significance versus fold change for differentially expressed genes between IR and Normal. (**C**) Gene Ontology (GO) enrichment analysis, highlighting significantly enriched terms in the Biological Process category. (**D**) KEGG pathway enrichment analysis, showing key pathways significantly enriched among the differentially expressed genes.

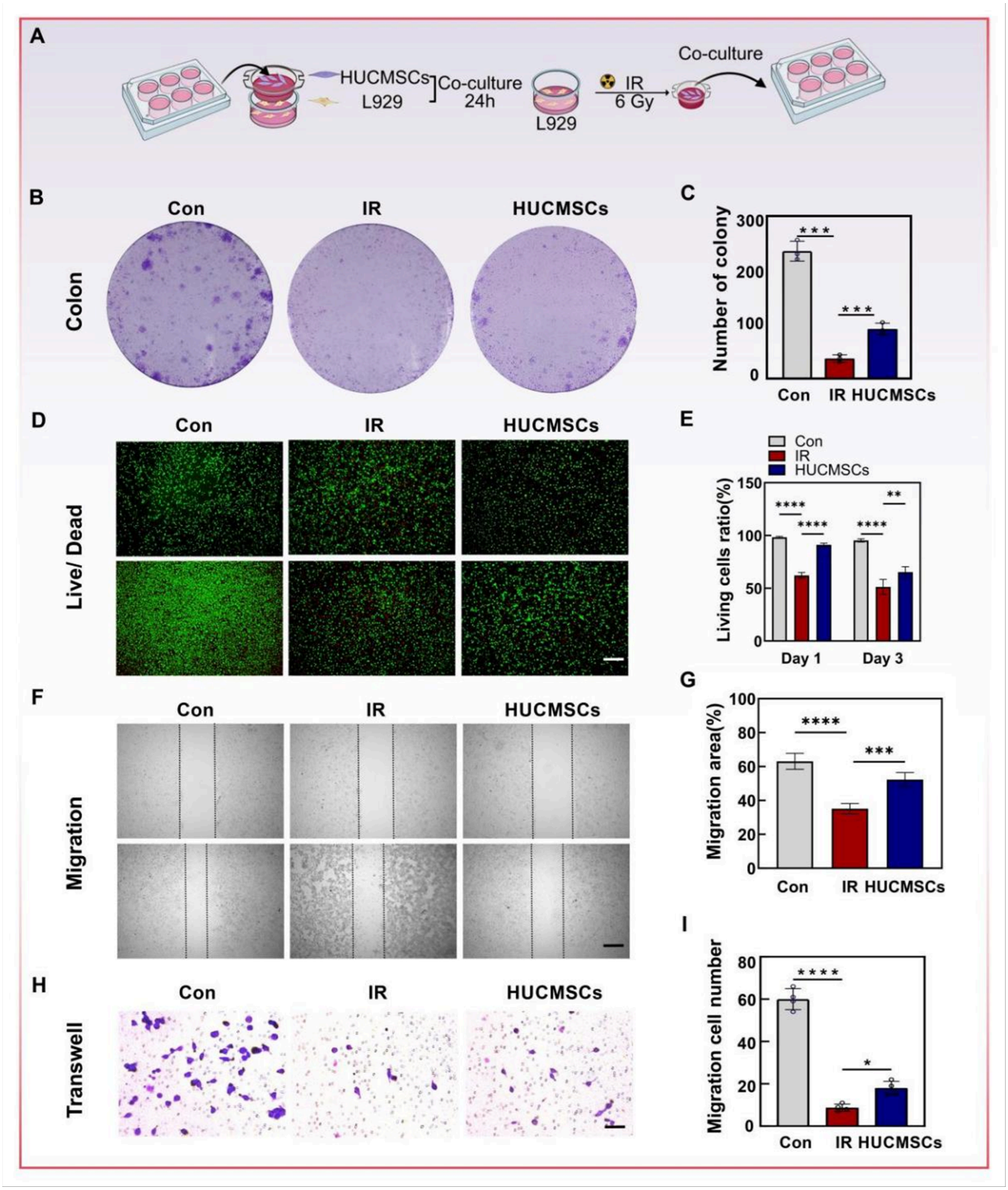

Figure 2

HUCMSCs promote proliferation and migration and restore function of irradiated L929 cells. (**A**) Schematic of the co-culture system used for HUCMSCs and irradiated L929 cells. (**B**) Representative colony formation images of irradiated L929 cells under different treatments. (**C**) Semi-quantitative analysis of colony numbers; n=3 (*p< 0.05, ***p < 0.001). (**D**) Representative Calcein-AM/PI fluorescence images; scale bar=100 μm. (**E**) CCK-8 cell viability assay showing relative viable cell rates for each group

post-irradiation; n=3 (**p< 0.01, ***p < 0.001). (**F**) Representative images from the scratch (wound-healing) assay comparing cell migration among groups; scale bars: 100 μm. (**G**) Semi-quantitative analysis of wound closure area (% closure); n=3 (***p< 0.001). (**H**) Representative images from Transwell migration assays; scale bar=50 μm. (**I**) Semi-quantitative analysis of migrated cells in Transwell assays; n=3 (***p < 0.001).

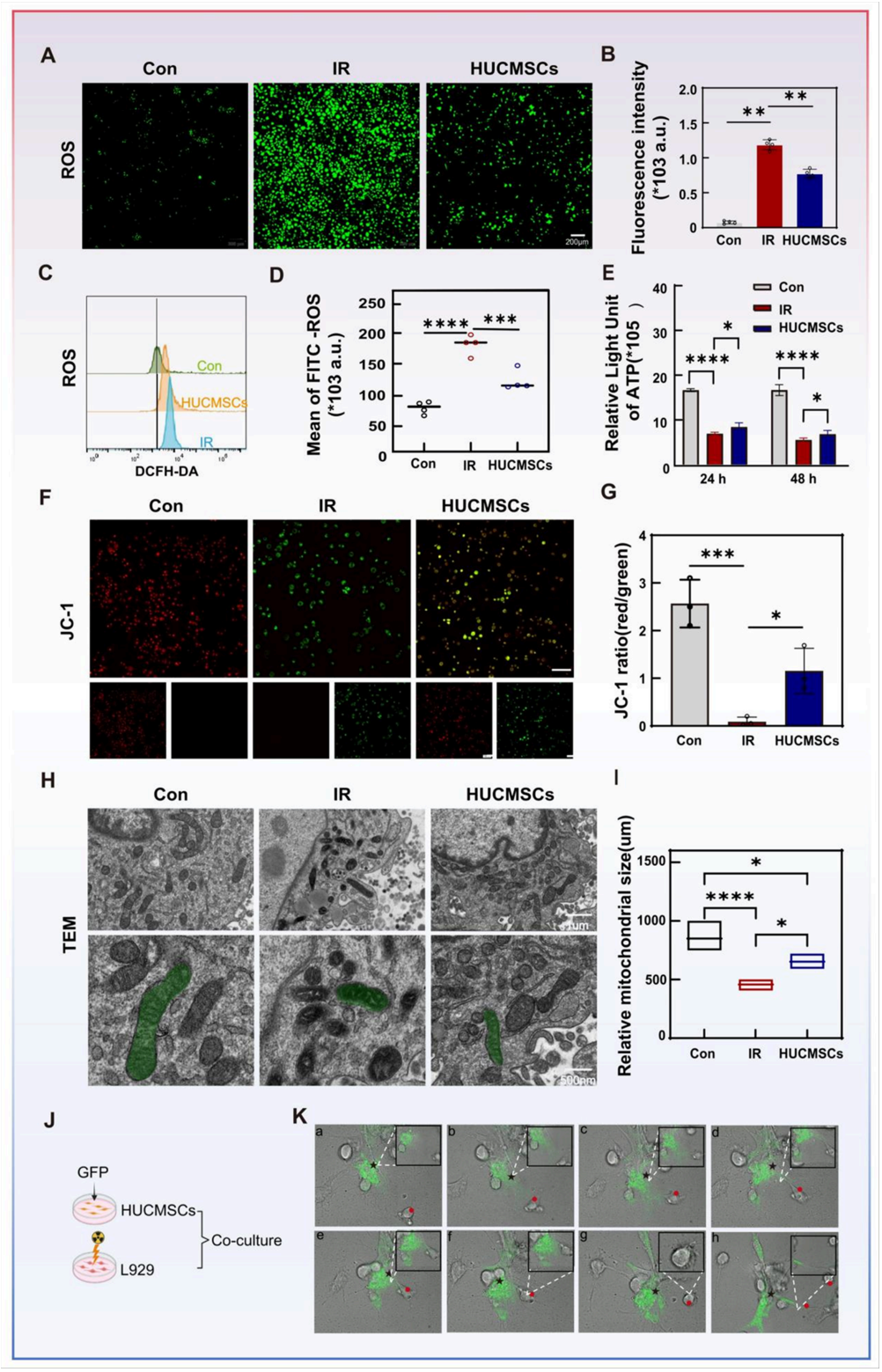

Figure 3

HUCMSCs mitigate irradiation-induced oxidative stress and mitochondrial alterations in L929 cells. (A) Representative DCFH-DA fluorescence images showing intracellular reactive oxygen species (ROS) levels in irradiated L929 cells across treatment groups; scale bar: 200 μm. **(B)**Semi-quantitative analysis of DCFH-DA fluorescence intensity; n=3 (**p<0.01). **(C)** Representative flow-cytometry plots of DCFH-DA fluorescence used to assess intracellular ROS. **(D)** Quantification of DCFH-DA fluorescence comparing intracellular ROS levels among groups. **(E)** ATP content measured in L929 cells at 24 h and 48 h post-irradiation across groups, n=5(*p<0.05, **p<0.01, ***p<0.001). **(F)** Representative JC-1 fluorescence images indicating mitochondrial membrane potential (MMP) differences among groups; scale bar: 200 μm. **(G)** Semi-quantitative analysis of JC-1 fluorescence signals to evaluate MMP; n=3(*p<0.05, ***p<0.001). **(H)** Representative transmission electron microscopy (TEM) images showing ultrastructural mitochondrial alterations in irradiated L929 cells. (I) Semi-quantitative analysis of mean mitochondrial length from TEM images. (J) Schematic of the assay to detect mitochondrial transfer during co-culture of GFP-labeled HUCMSCs with irradiated L929 cells. **(K)** Representative live confocal time-lapse images after 48 h of co-culture (Black indicates HUCMSCs and red indicates L929 cells).

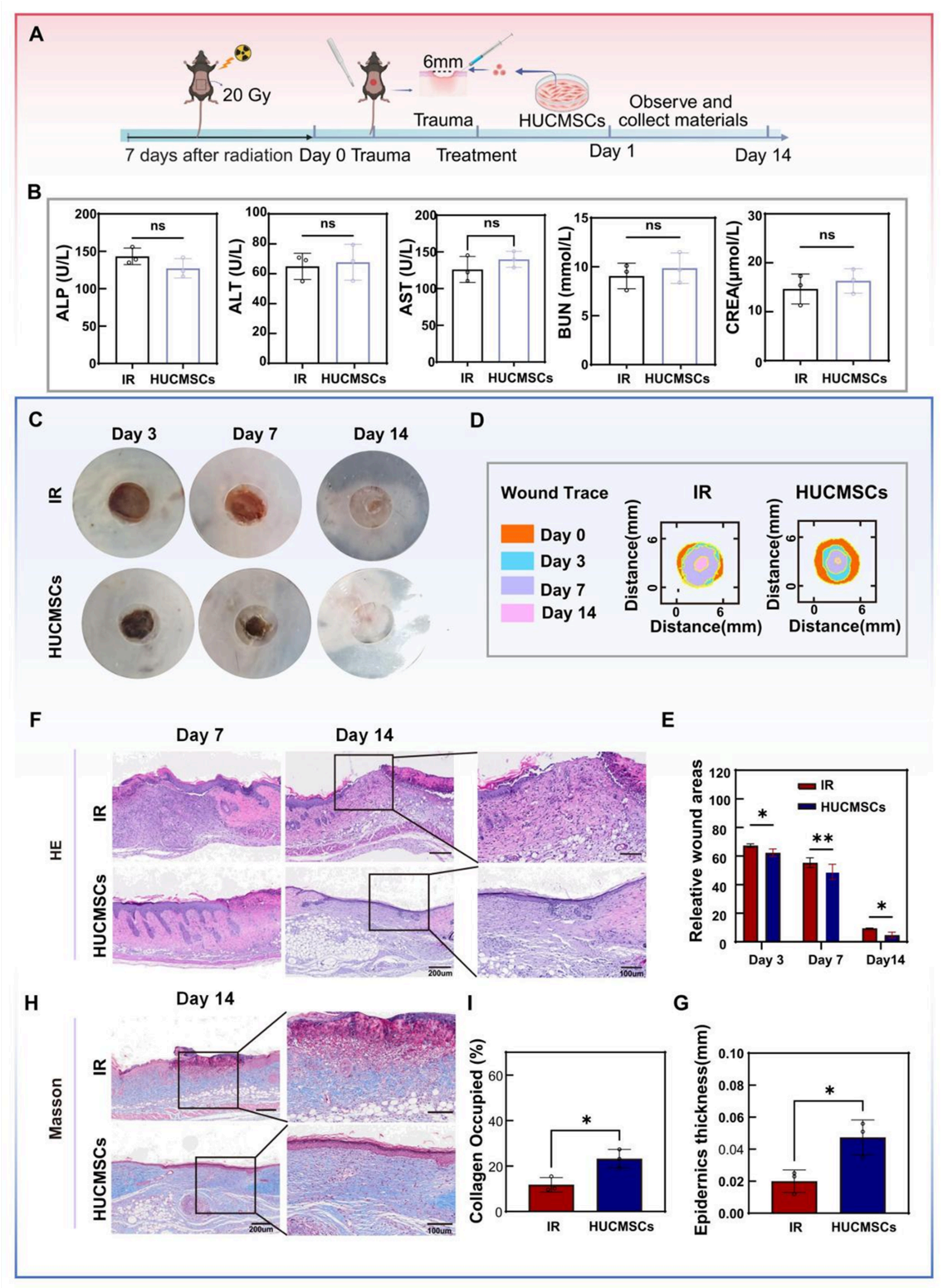

Figure 4

HUCMSCs accelerate wound healing in radiation-induced skin injury. (A) Schematic of the mouse radiation-induced skin injury model. **(B)**Safety evaluation following local HUCMSCs injection on Day 7 post-modeling. **(C)**Representative images of wounds from each group at Day 3, Day 7 and Day 14. **(D)**Overlay images of wound areas at Day 0, Day 3, Day 7 and Day 14 to illustrate healing progression. **(E)** Quantification of wound closure rates for each group at indicated time points (Day 3, Day 7, Day 14); n=3

(*p < 0.05, **p < 0.01). **(F)** Representative H&E staining of wound tissues at specified time points at Day 7 and Day 14; scale bars: 200 μm (top) and 100 μm (bottom). **(G)** Semi-quantitative analysis of epidermal regeneration thickness at Day 14; n=3 (*p < 0.05). **(H)** Representative Masson's trichrome staining of wound tissues at indicated time points; scale bars: 200 μm (top) and 100 μm (bottom). **(I)** Semi-quantitative analysis of collagen deposition based on Masson staining; n=3 (*p < 0.05).

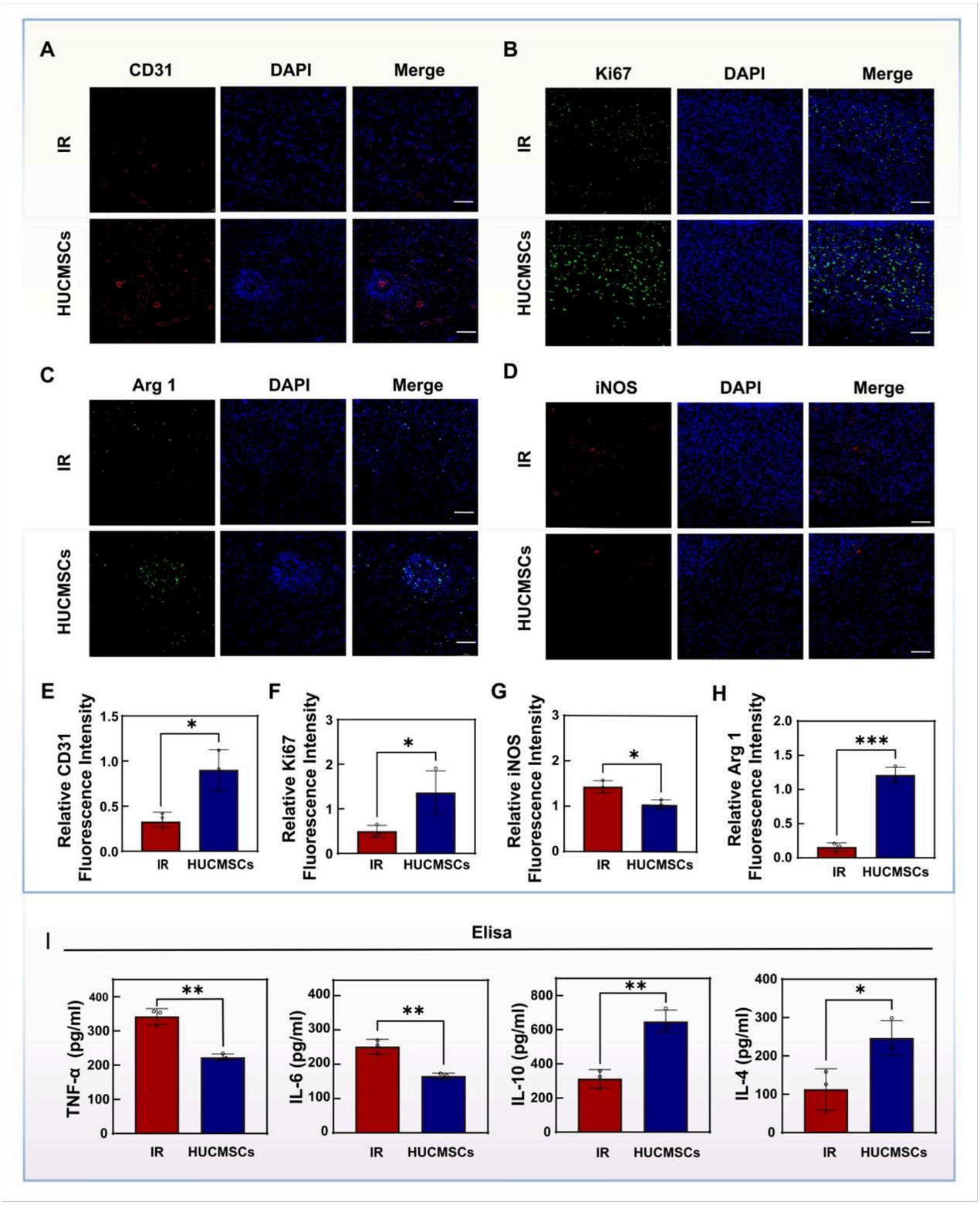

Figure 5

HUCMSCs enhance wound vascularization and attenuate inflammation. (A) Representative immunofluorescence image of CD31 showing vascular distribution in wound tissue. **(B)** Representative immunofluorescence image of Ki67 indicating cell proliferation in wound tissue. **(C)** Representative immunofluorescence image of iNOS and corresponding quantification to assess pro-inflammatory phenotype. **(D)** Representative immunofluorescence image of Arg1 showing distribution of alternatively activated/anti-inflammatory phenotype. **(E)** Semi-quantitative analysis of CD31 fluorescence intensity to compare vascularization among groups. **(F)** Semi-quantitative analysis of Ki67 fluorescence intensity to compare proliferative activity among groups. **(G)**Semi-quantitative analysis of iNOS fluorescence intensity to compare pro-inflammatory marker expression among groups. **(H)** Semi-quantitative analysis of Arg1 fluorescence intensity to compare anti-inflammatory marker expression among groups. **(I)** Elisa quantification of wound tissue Protein levels of TNF-α, IL-6, IL-10 and IL-4. n=3 (*p<0.05, **p<0.01, ***p<0.001). Scale bars: 50 μm.

Supplementary Files

This is a list of supplementary files associated with this preprint. Click to download.

- SupplementaryInformation.docx
- Graphicalabstract.docx